Journal of Nanobiotechnology

RESEARCH Open Access

A new strategy of using low-dose caffeic acid carbon nanodots for high resistance to poorly differentiated human papillary thyroid cancer

Jingwei Xin[1,2], Meiwei Song[1], Xiangling Liu[1], Hongrui Zou[2], Jifeng Wang[1], Lizhi Xiao[1], Yunxiao Jia[3*], Guoqi Zhang[4], Wei Jiang[3], Ming Lei[3], Yanyan Yang[2*] and Yingnan Jiang[1,5*]

Abstract

Thyroid cancer is one of the most common endocrine malignancies in clinical practice. Traditional surgery and radioactive iodine ablation have poor treatment results for poorly differentiated thyroid cancer, and there is a risk of metastasis and recurrence. In this study, caffeic acid, a natural herbal extract with certain biological activity, has been as precursor to prepare new caffeic acid carbon nanodots via a one-step hydrothermal method. The caffeic acid carbon nanodots retains part of the structure and biological activity of caffeic acid, and have good biocompatibility, water solubility and stability. The construction of the carbon nanodots could effectively improve their bio-absorption rate and the efficacy. In vitro cell experiments showed that low-dose caffeic acid carbon nanodots had a significant inhibitory effect on poorly differentiated papillary thyroid carcinoma BCPAP cells. At low concentrations of 16 μg/mL, the inhibition rate of human thyroid cancer cells BCPAP was ~ 79%. The anti-tumor mechanism was predicted and verified by transcriptome, real-time quantitative PCR and western blot experiments. The caffeic acid carbon nanodots showed to simultaneously downregulate the expression of KRAS, p-BRAF, p-MEK1 and p-ERK1/2, the four continuous key proteins in a MAPK classical signaling pathway. In vivo experiments further confirmed the caffeic acid carbon nanodots could significantly inhibit the tumorigenicity of xenografts in papillary thyroid carcinoma at quite low doses. This piece of work provides a new nanomedicine and therapeutic strategy for highly resistant poorly differentiated papillary thyroid carcinoma.

Keywords Herbal extract, Caffeic acid, Carbon nanodots, Nanomedicine, Poorly differentiated human papillary thyroid cancer

*Correspondence:
Yunxiao Jia
jyx811206@163.com
Yanyan Yang
yyy811128@jlu.edu.cn
Yingnan Jiang
jiangyn@ccucm.edu.cn
[1]Jilin Ginseng Academy, Changchun University of Chinese Medicine, Changchun 130117, China
[2]Jilin Provincial Key Laboratory of Surgical Translational Medicine, Division of Thyroid Surgery, China-Japan Union Hospital of Jilin University, Changchun 130033, China
[3]Department Gynecol & Obstet, Changchun Obstet Gynecol Hospital, Changchun Women and Children Health Hospital, Changchun 130042, China
[4]Harvard Medical School, Bonston Children's Hospital, Bonston 02111, US
[5]Australian Institute for Bioengineering and Nanotechnology , The University of Queensland, Brisbane, Queensland 4072, Australia

Introduction

Thyroid cancer is one of the most common malignancies in the endocrine system [1]. Over the past few decades, the incidence of thyroid cancer has been increasing rapidly worldwide [2–4]. Papillary thyroid carcinoma (PTC-1, BCPAP and K1) is the most common type of thyroid cancer, accounting for 85% ~ 90% of all thyroid cancers [5]. With the reduction of thyroid cancer differentiation (ATC, BCPAP and PDTC), conventional surgery and radioactive iodine ablation show poor treatment results for partially differentiated thyroid cancer. And the prognosis remains at risk of metastasis and recurrence [6]. Therefore, in order to provide more options for thyroid cancer therapy, improve the treatment effect of thyroid cancer, and inhibit the proliferation and migration of cancer cells, new drugs and treatment methods are always a research hotspot in the field of medicine worldwide.

It is well known that nanomedicines can overcome the therapy limitations of traditional small molecule drug in several ways. They could retain circulation in the blood for a longer time, accumulate at the tumor site through the enhanced permeability and retention (EPR) effect, utilize their nanoscale size and surface effect to be engulfed by cells at the lesion site, and greatly enhance the drug efficacy [7]. Carbon nanodots (CDs) are emerging zero-dimensional nanomaterials in recent years. They have the unique fluorescence excitation-dependent properties, good water solubility, excellent biocompatibility, high cell absorption, low toxicity, and environmental friendliness [8–21]. Thus, the CDs have developed rapidly in the field of nanomedicine, and have broad development prospects and clinical application value. Carbon dots are prepared from a wide range of raw materials, including organic small molecules, pharmaceutical small molecules, oligomers, natural herb and natural plant extracts. Attractively, some studies have confirmed that the CDs prepared based on the precursors with biological activities may preserve part of the structure and drug activity of the precursors. Moreover, owing to the unique nanosize effect and abundant surface functional groups, the CDs may be endowed with better or new drug activities, such as antibacterial, antitumor and anti-inflammatory activities [11–23]. Our group have proposed a nanomedicine ginsenosides carbon nanodots (GS-CDs) using natural bioactive molecules ginsenosides as the sole source. The GS-CDs retained part of the structure and efficacy of the original ginsenosides, and exerted a high inhibitory effect on human neuroblastoma SH-SY5Y cells, by taking advantage of its abundant hydrophilic functional groups and nanosize effects [19]. Zhang et al. prepared non-toxic PCC-CDs using the natural herb phellodendron as the sole precursor, which may be an anti-psoriasis drug candidate for clinical application in the treatment of psoriasis [21]. Yao group reported a major bioactive natural product from coffee, chlorogenic acid as the precursor to fabricate biocompatible nanozyme ChA CQDs. The ChA CQDs can be used for anticancer therapeutics [22].

Natural herbs are abundant and widespread in nature. The low-toxic active ingredients isolated and extracted from natural plants have many amazing drug activities, including anticancer, antioxidant, anti-inflammatory, and so on [24, 25]. Unfortunately, these natural herbs and herbal extracts are found to be difficult to permeate cell membranes in their molecular state. This results in low cell absorption, poor bioavailability, and poor therapeutic efficacy. However, a large increase in the concentration of these drugs may still show unsatisfactory therapeutic effects, while toxic side effects on human organs during absorption, degradation, metabolism, and excretion will inevitably occur [26].

Take caffeic acid (CA) as an example. CA has a wide range of sources in nature and is distributed in a variety of herbal plants such as cimicifuga, yinchen, eucommia, honeysuckle, etc. The main drug form of CA in clinical practice is caffeic acid tablets, which are often used to prevent bleeding or stop bleeding during surgery. In fact, CA may have other biological activities. For example, Luana et al. found that at a concentration of 1000 μg/mL, CA decreased the cell viability of human CM cells (SK-Mel-28) and induced the cell apoptosis. It suggested that CA may have some antitumor effects [27]. Yet, at such a high drug concentration, the inhibition rate of the cancer cells only reached to 50 ~ 60%. Apparently, due to its low water solubility, low cell absorption rate and poor bioavailability, the active CA is limited in experimental research and clinical application.

In this study, the CA-CDs were rapidly prepared by a hydrothermal method using caffeic acid, a natural plant active ingredient, as the only reactant (Scheme 1). The CA-CDs have good fluorescence properties, water solubility and biocompatibility. The construction of the CDs could effectively improve the bio-absorption rate and the efficacy of the anticancer drug. In vitro and in vivo experiments have shown that the CA-CDs had significant inhibitory effect on both poorly differentiated human papillary thyroid carcinoma cells (BCPAP) and poorly differentiated human papillary thyroid carcinoma at very low doses.

The anti-tumor mechanism of the CA-CDs was predicted and verified by transcriptome, real-time quantitative PCR (RT-qPCR) and western blot (WB) experiments. Remarkably, the CA-CDs has been shown to effectively downregulate the expression of KRAS, p-BRAF, p-MEK1 and p-ERK1/2, the four consecutive key proteins in the MAPK classical signaling pathway. The MAPK classical pathway plays an important role in cell proliferation, growth, differentiation and apoptosis, and is the hardest hit area for inducing tumor production. The MAPK

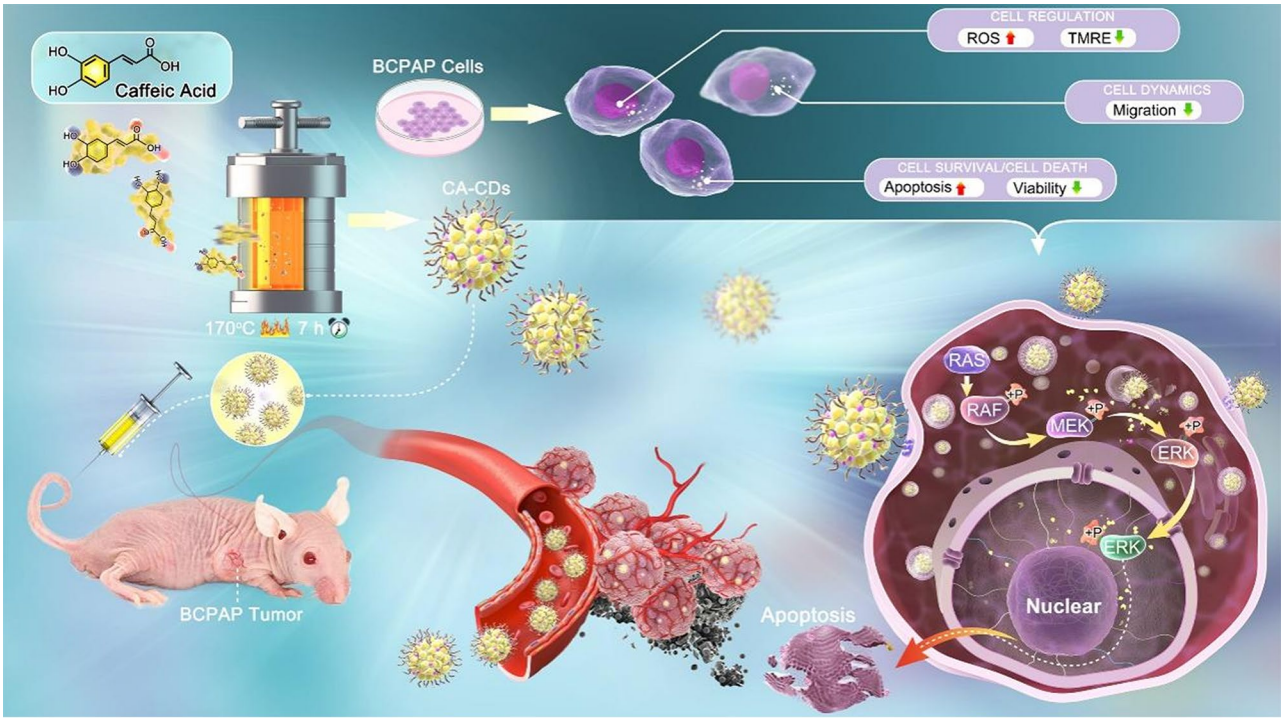

Scheme 1 Schematic synthesis route of the CA-CDs and their high inhibitory effect on poorly differentiated human thyroid cancer through a MAPK classic pathway

classical signaling pathway has a three-level signaling process, which activates receptor tyrosine kinases through growth factors and various extracellular signals, and sequentially activates RAS–RAF–MEK–ERK proteins to promote tumorigenesis [28, 29]. Therefore, this MAPK classical signaling pathway is closely related to the occurrence of a variety of cancers [30]. The RAS, RAF, MEK, and ERK proteins are the key targets in this pathway. Dysfunction of any one of these proteins can lead to serious oncological disease. In many previous anti-tumor studies, drugs that usually had a down-regulated effect on the expression of only one or two of these proteins can be considered as a strategy for tumor treatment. And several drugs for these key targets in this pathway have been successfully marketed [31–34]. Therefore, the CA-CDs (low dose) can be regarded as a perspective nanodrugs for the clinical treatment of poorly differentiated papillary thyroid carcinoma in the future.

Results and discussion

Characterization of the CA-CDs

The CA solution was transparent and showed little fluorescence under 365 nm UV lamp, while the prepared CA-CDs solution was pale yellow under light and showed yellow-green fluorescence under 365 nm UV irradiation (Fig. S1). Transmission electron microscopy (TEM) image showed that the CA-CDs had relative uniform size and good dispersion, with an average size of 9.70±0.10 nm (Fig. 1A and B). The CA-CDs exhibited excitation-dependent characteristics (Fig. 1C). At the optimal excitation wavelength of ~360 nm, the emission wavelength of the CA-CDs was ~420 nm. The fluorescence decay curve of the CA-CDs was fitted according to the second-order decay index function (Fig. 1D). Two fluorescence lifetimes (τ) were obtained, indicating that the CA-CDs had two fluorescence centers (Table S1). The average lifetime of the CA-CDs was ~3.24 nm and the quantum yield was ~0.8%.

The CA solution had three absorption peaks at ~216 nm, ~ 291 nm, and ~314 nm, respectively (Fig. 1E), indicating the presence of benzene ring and conjugated carbonyl group in the compound. The wide absorption at ~258 nm and the absorption peak at ~280 nm of the CA-CDs solution revealed the presence of π–π*, n–π* electronic transitions, indicating the presence of C=C, C=O, and C-O on the CA-CDs surface [35]. Fourier transform infrared spectroscopy (FTIR) showed that CA had absorption peaks at 3417, 3228, 1639, 1524, 1293, 1210 and 1117 cm^{-1}, which were related to the expansion and contraction vibrations of the functional groups O-H, C-H, C=O, C=C and C-O (Fig. 1F). While for the CA-CDs, the absorption peak at ~3380 cm^{-1} belonged to the expansion vibration of O-H bond, the absorption peak at ~2920 cm^{-1} belonged to the presence of C-H bond, the absorption at ~1600 cm^{-1} belonged to the expansion vibration of C=O, the absorption at ~1500 cm^{-1} was

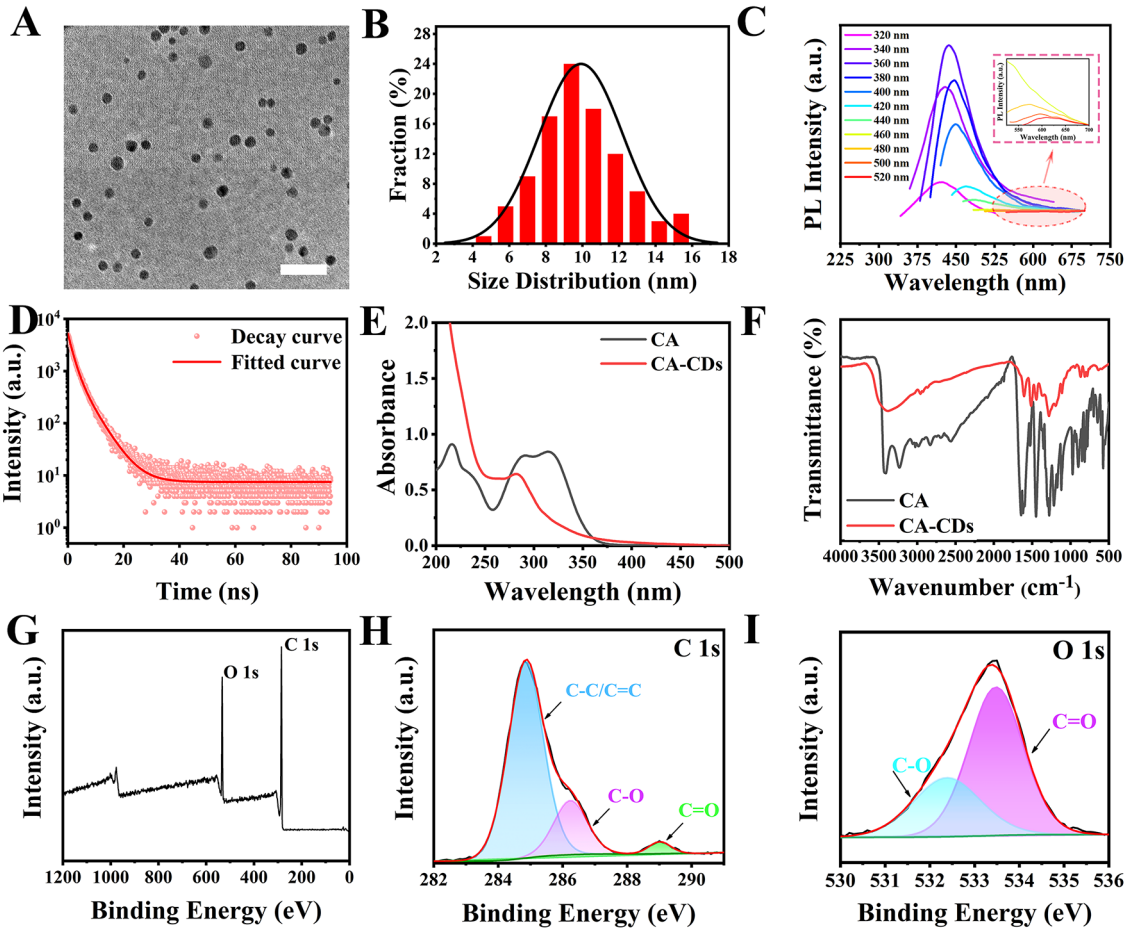

Fig. 1 Structural characterization of the CA-CDs. (**A**) (**B**) TEM image and size distribution of the CA-CDs, the scale bar was 50 nm. (**C**) Fluorescence spectra of the CA-CDs at different excitation wavelengths of 320 ~ 520 nm. (**D**) Fluorescence attenuation curve of the CA-CDs. (**E**) UV-Vis absorption spectra of CA and the CA-CDs (0.2 mg/mL) in aqueous solution. (**F**) FT-IR spectra of CA and the CA-CDs. (**G**) High-resolution XPS spectra of the CA-CDs: C1s spectra (**H**) and O1s spectra (**I**)

the expansion vibration of benzene ring skeleton, and the absorption at ~ 1196 cm^{-1} was the expansion vibration of C-O. XPS full-spectra scan showed that both CA and the CA-CDs were composed of C and O elements (Fig. S2 and Fig. 1G). The high-resolution C1s spectra of the CA-CDs had distinct peaks at 284.8 eV, 286.3 eV, and 288.5 eV, which related to the presence of C=C/C-C, C-O, and C=O, respectively (Fig. 1H) [36]. The characteristic peaks at ~ 531.9 eV and ~ 533.5 eV in the high-resolution O1s spectra correspond to the C-O and C=O groups, respectively (Fig. 1I). The atomic ratios of C and O in CA were ~ 71.65% and ~ 28.35%. The corresponding atomic ratios of the CA-CDs were ~ 78.14% and ~ 21.86%. It suggested that hydrothermal synthesis caused the partial chemical bonds of CA to break and reassemble during the fabrication of the CA-CDs. The change in the atomic ratio was the result of the formation of CDs through carbonization [37]. The above results indicated that the CA-CDs retained part of the structure of CA, and the surface was rich in -OH and -COOH groups.

The stability of nanomedicine is an important indicator to measure whether it can be applied. First, the stability of the CA-CDs in a wide concentration range of NaCl (0–1.0 mol/L) and KCl (0–1.0 mol/L) was tested. It can be seen that the increase in NaCl and KCl concentrations hardly affected the fluorescence intensity of the CA-CDs (Fig. S3A and S3B). The results showed that the CA-CDs had good salt resistance, and their structure and properties would be less affected in organisms (the concentration of normal salts in normal body fluids is ~ 0.15 mol/L). The CA-CDs were irradiated at 365 nm ultraviolet for 180 min. The fluorescence intensity of the CA-CDs also changed little, implying that the CA-CDs had good photobleaching resistance (Fig. S3C). In addition, considering the use of the CA-CDs is as a drug, the stability had been also tested in the phosphate-buffered saline, RPMI 1640 media, fetal bovine serum and penictomycin mixture (Fig. S4). There were some little changes of the fluorescence properties of the CA-CDs.

It suggested that the CA-CDs were stable in complicated bioenvironments.

In vitro inhibition effect of the CA-CDs on BCPAP cells

Based on the above good physical and chemical properties of the CA-CDs, the biological activity of the CA-CDs in vitro was studied by Cell-Counting-Kit-8 method (CCK-8). After 48 h of co-incubation, low-dose CA-CDs showed a significant inhibitory effect on the proliferation of the papillary thyroid cancer cells BCPAP (Fig. 2A). As the dosing concentration increased, the cell viability decreased obviously. At concentrations of 12 μg/mL and 16 μg/mL of the CA-CDs, inhibition rate of the BCPAP cells reached ~ 73% and ~ 79%, respectively. In contrast, CA showed little effect on the cell viability of the BCPAP cells (Fig. 2B). As a natural herbal medicine, CA should have many biological activities. However, due to the poor water solubility and low cell membrane permeability of CA molecules, the bioavailability and medicinal value of CA molecules have been seriously hindered. The above experiments have demonstrated that the CA-CDs had certain hydrophilic groups on the surface, could be uniformly dispersed in water, and retained part of the structural of CA. Thus, the CA-CDs may possess certain biological activity. When the CA-CDs were co-incubated with the BCPAP cells, they can be engulfed through the

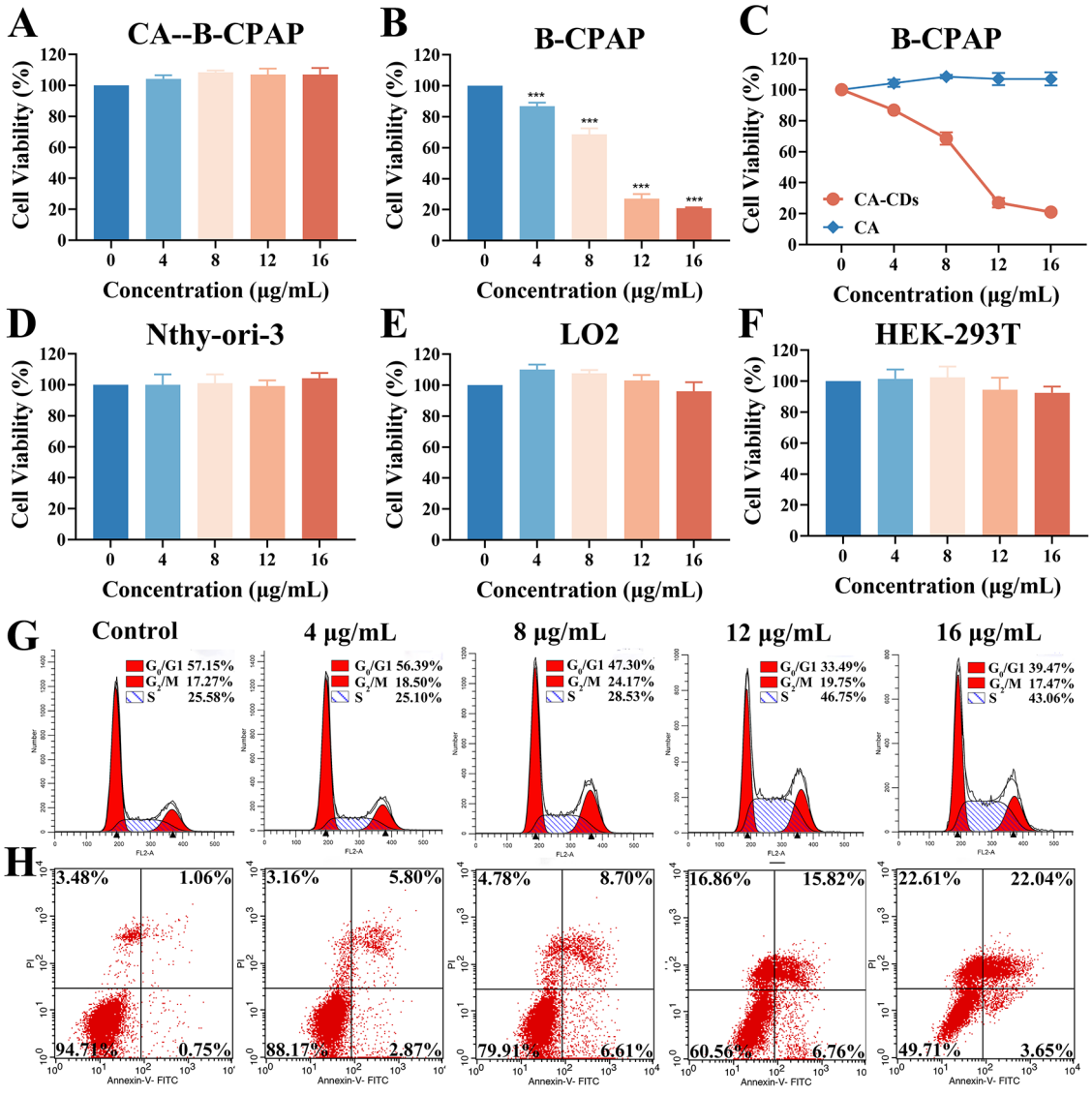

Fig. 2 Effects of the CA-CDs on viability, cycle, and apoptosis of the BCPAP cells. (**A**) Effect of the CA-CDs on the viability of the BCPAP cells. (**B**) Effect of CA on the BCPAP cell viability. (**C**) Statistic diagram comparing the effects of CA and the CA-CDs on the BCPAP cell activity. Effect of the CA-CDs on the cell activity of Nthy-ori-3 (**D**), LO2 (**E**) and HEK-293T (**F**). (**G**) .Flow cytometry cycle diagram of the BCPAP cells after 48 h treatment with the CA-CDs (0 μg/mL, 4 μg/mL, 8 μg/mL, 12 μg/mL and 16 μg/mL). (**H**) Apoptosis of the BCPAP cells after 48 h treatment with the CA-CDs (0 μg/mL, 4 μg/mL, 8 μg/mL, 12 μg/mL and 16 μg/mL). *$p < 0.05$; **$p < 0.01$; ***$p < 0.001$ compared to Control

cells in large quantities owing to their nanometer size and surface functional groups, and thereby exerted efficient drug effects (Fig. 2C) [7, 8]. In addition, CCK-8 analysis demonstrated low biotoxicity of the CA-CDs on normal thyroid cells Nthy-ori-3, hepatic normal cells LO2, and renal normal cells HEK-293T under the same conditions (Fig. 2D, E and F). These results suggested that the CA-CDs could be considered as a potential nanodrug against papillary thyroid carcinoma.

The cell cycle is closely related to cell proliferation. Flow cytometry showed that most of the BCPAP cells of Contral group (CA-CDs 0 μg/mL) were in the G0/G1 phase, with fewer cells in the S phase and the smallest proportion of cells in the G2/M phase. The proportion of S phase of the BCPAP cells increased after 48 h treated with different concentrations of the CA-CDs (4 μg/mL, 8 μg/mL, 12 μg/mL and 16 μg/mL) (Table S2). In particular, after treatment with the CA-CDs at concentrations of 12 μg/mL and 16 μg/mL, the proportion of the BCPAP cells in S phase was as high as ~46% and ~43% ($p<0.001$, $p<0.01$), indicating that the CA-CDs could arrest the BCPAP cells in S phase (Fig. 2G). After 48 h of incubation with the CA-CDs (4 μg/mL, 8 μg/mL, 12 μg/mL and 16 μg/mL), the apoptosis of the BCPAP cells was detected by a flow cytometry. The proportion of early apoptosis and late apoptosis of the BCPAP cells in the Contral group (CA-CDs 0 μg/mL) was ~1.07% and ~1.58%, respectively. The proportion of early apoptosis and late apoptosis of the BCPAP cells in the maximum administration treatment group (CA-CDs 16 μg/mL) was ~5.31% and ~30.16%, respectively (Table S3), indicating the significantly increase of apoptosis rate ($p<0.05$, $p<0.001$). The results showed that the low-dose CA-CDs could significantly induce the BCPAP apoptosis, and the apoptosis rate was positively correlated with the dose of the CA-CDs (Fig. 2H).

In order to further explore the inhibitory effect of the CA-CDs on the BCPAP cells, the entry of the CA-CDs into the BCPAP cells at different incubation times was monitored by fluorescence microscopy (Fig. 3). In brightfield, it could be seen that with the extension of incubation time, the BCPAP cells gradually shrank and became rounded, and the cell morphology was disrupted. It can be seen that the CA-CDs can effectively enter the cells and emitted green and red fluorescence under different light irradiation. After co-incubation for 0 ~ 24 h, the fluorescence intensity of the system gradually increased, indicating that the number of intracellular CA-CDs increased with time. The fluorescence intensity of the system was the highest at 24 h, indicating that the BCPAP cells had the highest uptake of the CA-CDs. From 24 to 48 h, the fluorescence intensity of the system decreased, and the fluorescence was almost undetectable at 48 h. This may be due to the structural destruction of

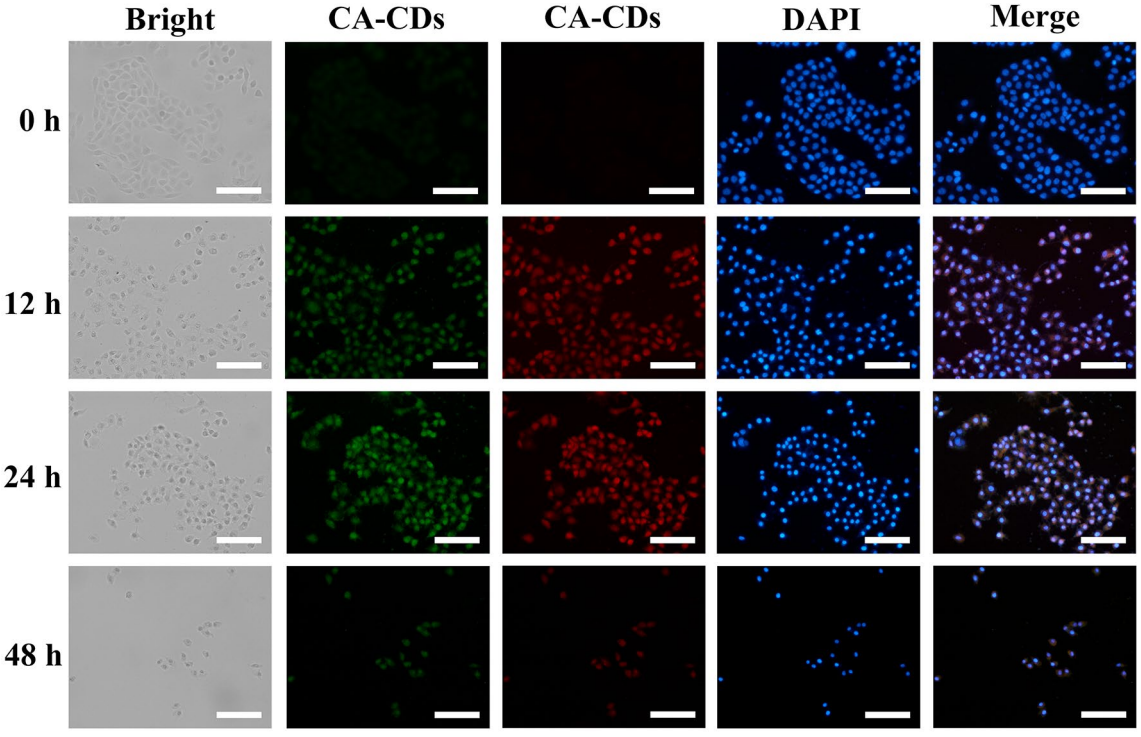

Fig. 3 Distribution of the CA-CDs in BCPAP cells with time. Fluorescence microscopy images of the CA-CDs (30 μg/mL) and the BCPCP cells under brightfield and fluorescence fields (fluorescence excitation wavelengths 488 nm, 405 nm and 516 nm) after co-incubation for different times (0 h, 12 h, 24 h and 48 h). The scale bars were 100 μm

the intracellular CA-CDs by reacting with the cell matrix, accompanied with the gradual shrinkage and death of the BCPAP cells. The change of fluorescence intensity in the incubation system suggested that the inhibitory effect of the CA-CDs on the BCPAP cells was time-dependent. In addition, the uptake of the CA-CDs by the LO2 cells and the Nthy-ori-3 cells at different times was also observed (Fig. S5 and S6). The LO2 cells and the Nthy-ori-3 cells exhibited similar uptake properties of the CA-CDs, compared with the BCPAP cells. It implies that the CA-CDs can also be taken up by the normal cells, but performed little inhibition on these cells.

Reactive oxygen species (ROS) are also an important factor in cancer treatment research. Elevated ROS levels can induce apoptosis through both endogenous and exogenous pathways. Here, the changes in ROS fluorescence intensity in the BCPAP cells after treated with different concentrations of the CA-CDs (4, 8, 12, and 16 μg/mL) were observed by fluorescence microscopy (Fig. 4A). Compared with the control group (0 μg/mL CA-CDs), the average intracellular ROS red fluorescence intensity was much stronger when the concentration of the CA-CDs reached 12 μg/mL ($p<0.01$). When the concentration of the CA-CDs reached 16 μg/mL, the intracellular

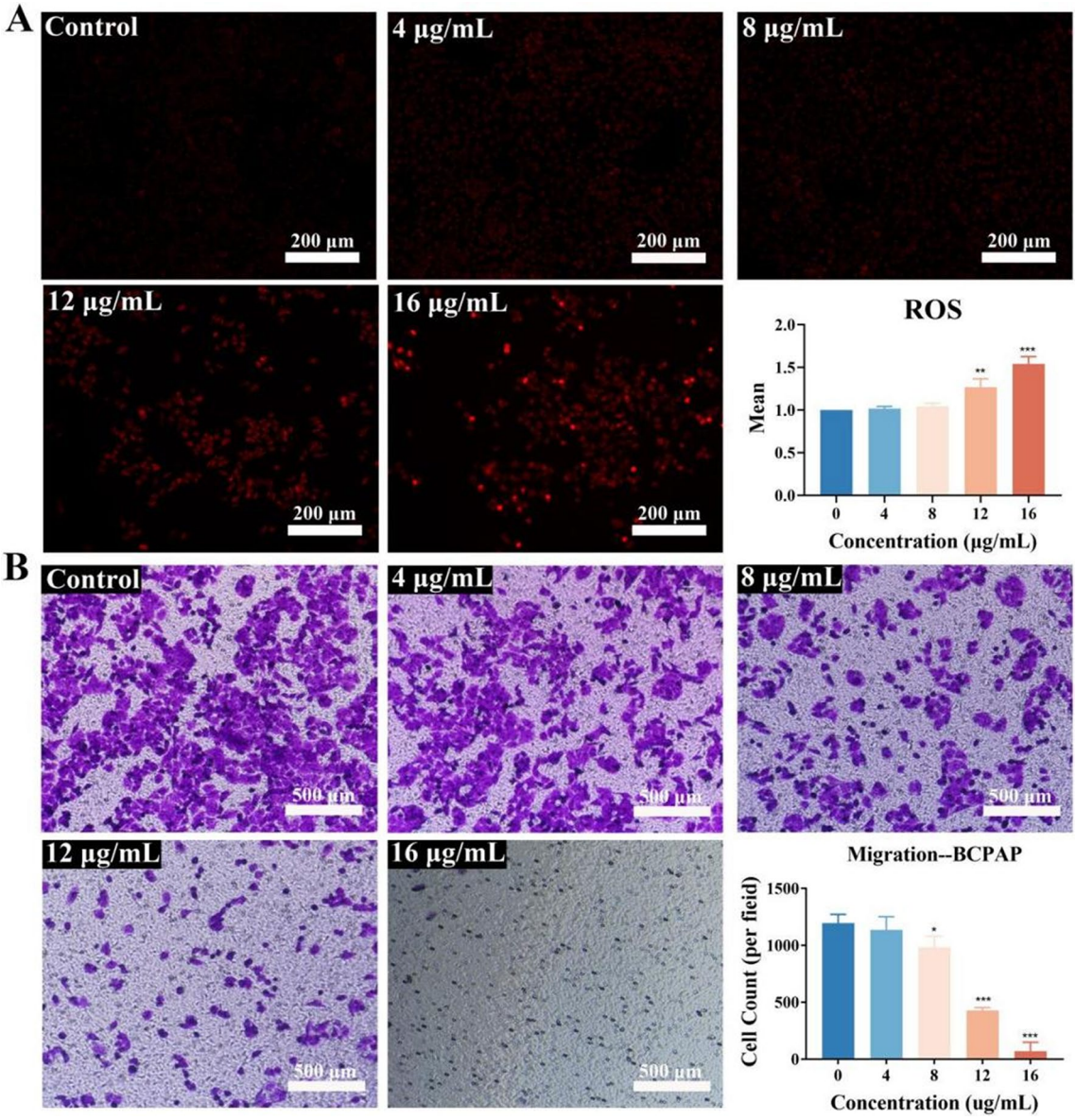

Fig. 4 (**A**) After 48 h of treatment with different concentrations of the CA-CDs, the fluorescence photos of ROS in the BCPAP cells and the corresponding mean fluorescence intensity change quantitative column chart. The scale bars were 200 μm. (**B**) Migration and invasion dyed images of the BCPAP cells, and the corresponding statistic diagram of the number of migrating cells after 48 h treatment with different concentrations of the CA-CDs. The scale bars were 500 μm. *$p<0.05$; **$p<0.01$; ***$p<0.001$ compared to Control

ROS red fluorescence was further significantly enhanced. The images in brightfield also showed that with the increase of the CA-CDs administered concentration, the morphology of the BCPAP cells shrunk and rounded, and the number of the cells decreased obviously (Fig. S7). These results showed that the CA-CDs could inhibit the BCPAP cells by triggering a large amount of ROS production in cells. After 48 h of treatment with the CA-CDs (0, 4, 8, 12, and 16 μg/mL), the mitochondrial membrane potential (MMP) changes of the BCPAP cells were observed by fluorescence microscopy (Fig. S8). It was found that the MMP orange-red fluorescence intensity in the BCPAP cells decreased significantly after 16 μg/mL CA-CDs treatment.

The transwell assay was used to evaluate the effects of the CA-CDs on the migration and invasion of the BCPAP cells (Fig. 4B). Compared with the control group (CA-CDs, 0 μg/mL), the migration and invasion ability of the BCPAP cells was significantly reduced after treatment with different concentrations of the CA-CDs (4 μg/mL, 8 μg/mL, 12 μg/mL and 16 μg/mL). When the concentration of the CA-CDs reached 12 and 16 μg/mL, the migration and invasion ability of the BCPAP cells was inhibited by ~65% and ~94%, respectively ($p<0.001$). It suggested the CA-CDs could significantly and effectively weaken the migration and invasion ability of the BCPAP cells, which might reduce the possibility of cancer cell metastasis and spread.

Effect of the CA-CDs on the expression of MAPK pathway-related proteins in the BCPAP cells

After 48 h treatment of the BCPAP cells with the CA-CDs (16 μg/mL), transcriptomics analysis was performed between the CA-CDs group (CA-CDs 16 μg/mL) and the Control group (CA-CDs, 0 μg/mL). A volcano plot of transcriptome differential gene screening results between the CA-CDs group ($n=5$) and the Control group ($n=5$) were plotted (Fig. 5A). Compared with the Control group, 7596 differential genes were screened out in the CA-CDs group. Among them, 2783 genes were up-regulated and 4813 genes were down-regulated. The two groups of differential genes (SOS1, KRAS, BRAF, MAPK1, ELK1, GCNT3 and HSPA6) were randomly selected for correlation analysis. It was found that the data of the two groups ($n=5$) were reproducible and there were differences between the groups, which could be used for subsequent analysis (Fig. 5B). For the aim to test the data reliability of the transcriptome, the randomly selected differential

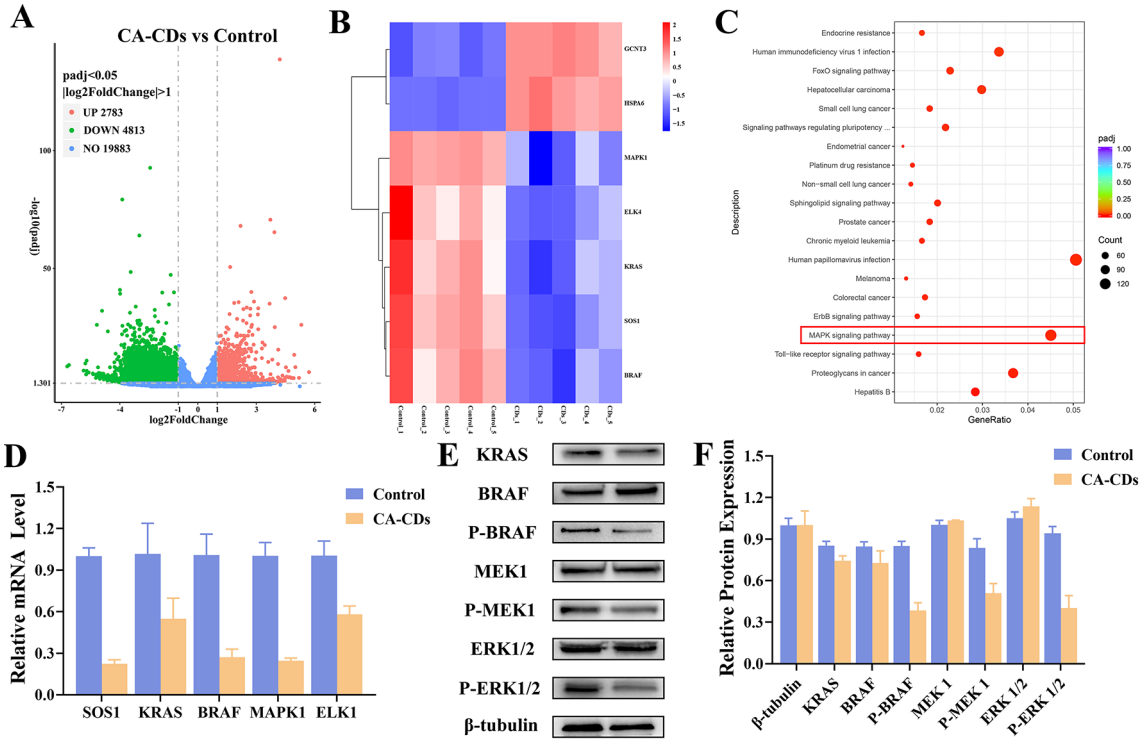

Fig. 5 Anti-tumor mechanism experiments of the CA-CDs treated the BCPAP cells after 48 h. (**A**) A volcano plot of transcriptome differential gene screening results of CA-CDs group and Control group ($n=5$). Green dots represent down-regulated genes, and red dots represent up-regulated genes. (**B**) Data correlation analysis heat map of CA-CDs group and Control group ($n=5$). (**C**) Bubble map of the top 20 KEGG pathways with the highest differential gene enrichment. (**D**) The relative mRNA levels of SOS1, KRAS, BRAF, MAPK1 and ELK1 genes in BCPAP cells in CA-CDs group and Control group, detected by qRT-PCR. (**E**) WB images of MAPK classical pathway-related proteins of BCPAP cells in CA-CDs group and Control group. The Control group was on the left and the CA-CDs group was on the right. (**F**) The statistic histogram of relative protein expression

genes SOS1, KRAS, BRAF, MAPK1 and ELK1 in Fig. 5B were verified by qRT-PCR (Fig. 5D). It can be seen that the down-regulation trend of these five genes was obvious, which was consistent with the trend of transcriptome sequencing analysis in Fig. 5B. KEGG enrichment analysis was performed on all differential genes, and the top 20 KEGG pathways with the highest enrichment were selected for plotting (Fig. 5C). The signaling pathways with a high degree of differential gene enrichment were Human papillomavirus infection, mitogen-activated protein kinase (MAPK) signaling pathway, proteoglycans in cancer and human immunodeficiency virus 1 infection.

The WB was used to analyze the regulatory effect of the CA-CDs on the MAPK classical signaling pathway in the BCPAP cells (Fig. 5E and F). Compared with the Control group, there was little expression content change in the BRAF, MEK1 and ERK1/2 proteins in the BCPAP cells, while the expression contents of KRAS, p-BRAF, p-MEK1 and p-ERK1/2 proteins were significantly reduced. It is speculated that the CA-CDs could simultaneously inhibit the proliferation of the BCPAP cells and promote the apoptosis of the BCPAP cells by inhibiting the expression of the continuous RAS–RAF–MEK–ERK proteins in the MAPK classical signaling pathway.

Inhibitory effect of the CA-CDs on poorly differentiated human papillary thyroid tumors in vivo

BCPAP cells were injected into the subcutaneous skin of BALB/c nude mice, and a xenogeneic tumor-bearing model was established. The tumor-bearing nude mice were randomly selected to three groups ($n=5$) and injected through the tail vein: the normal saline (90 mg/kg, 5 times per week) as the Model group; the CA-CDs (2 mg/kg, 5 times per week) as the CA-CDs group; the clinical anti-thyroid tumor drug cyclophosphamide (CTX, 60 mg/kg, 3 times per week) was used as the CTX group. Normal mice were injected with normal saline (90 mg/kg, 5 times per week) in the tail vein as the Control group ($n=5$). Normal mice were injected with the CA-CDs (2 mg/kg, 5 times per week) in the tail vein as the Control + CA-CDs group ($n=5$). Under the same feeding condition, the experimental cycle was set 14 days, within which observed the indicators of the mice. On the 14th day, the subcutaneous tumors of nude mice were removed for detection and analysis. Compared with the Model group, the tumor volume and weight of mice in the CTX group and the CA-CDs group were significantly reduced (Fig. 6A, B and C). The tumor volume of mice in the CA-CDs group decreased more, compared with that in the CTX group (Fig. 6C). The results indicated that low-dose CA-CDs had a good inhibitory effect on human papillary thyroid tumors, and the inhibitory effect was better than that of the positive control CTX.

The body weight changes of mice in the Model group, Control group, CTX group, CA-CDs group, and Control + CA-CDs group were recorded to evaluate the safety of CA-CDs. The mice in the Control group, Control + CA-CDs group, Model group and CA-CDs group were in good condition, and their body weight was steadily increasing (Fig. 6D). The mice in the CTX group became malaise after injection with the drug, and their body weight was clearly lower than that of the mice in other groups. The body weight of mice in the Control + CA-CDs group was higher than that in the Control group. This also indicated that the CA-CDs had low toxicity and side effects to organism, and had good biological safety. On the 14th day, the major organs (heart, liver, spleen, lung, and kidney) of mice in each group were collected for histological analysis to evaluate pathological differences (Fig. S9). Compared with the Control group, there was little organ damage and inflammatory damage in the main organs of the mice in the CA-CDs group and the Control + CA-CDs group. It further demonstrated that the CA-CDs may have good biocompatibility in vivo.

H&E staining was used to observe the damage of human papillary thyroid tumor tissue in mice in each group (Fig. 6E). H&E staining showed that the tumor cells of mice in the Model group were tightly arranged and there were fewer apoptotic cells. A large number of apoptotic cells appeared in the tumor tissues of mice in the CTX group and the CA-CDs group. The cells were loosely arranged, and the number of apoptotic cells was significantly higher than that of the Model group. These results indicated that high-dose CTX and low-dose CA-CDs could promote tumor tissue necrosis. Tunel method is widely used to detect apoptosis in tissue sections. Tunel staining showed that the tumor cells of mice in the Model group were tightly arranged and blue, and apoptotic cells with brownish-yellow nuclei were almost absent. The tumor cells of the mice in the CA-CDs group were loosely arranged, the cell volume was small, and most of the cells were brown. The tumor cells of the mice in the CTX group were not much different from those in the CA-CDs group (Fig. 6E). The expression of markers related to differentiation and proliferation (CDK4 protein and Ki-67 protein markers) in human papillary thyroid tumors in each group was observed by immunohistochemistry (IHC) (Fig. 6E). The results showed that the CDK4 and Ki-67 were highly expressed in the Model group, moderately expressed in the CTX group, and lightly expressed in the CA-CDs group. The above results suggested that low-dose CA-CDs could promote apoptosis and inhibit cell proliferation in human papillary thyroid tumor tissues in vivo.

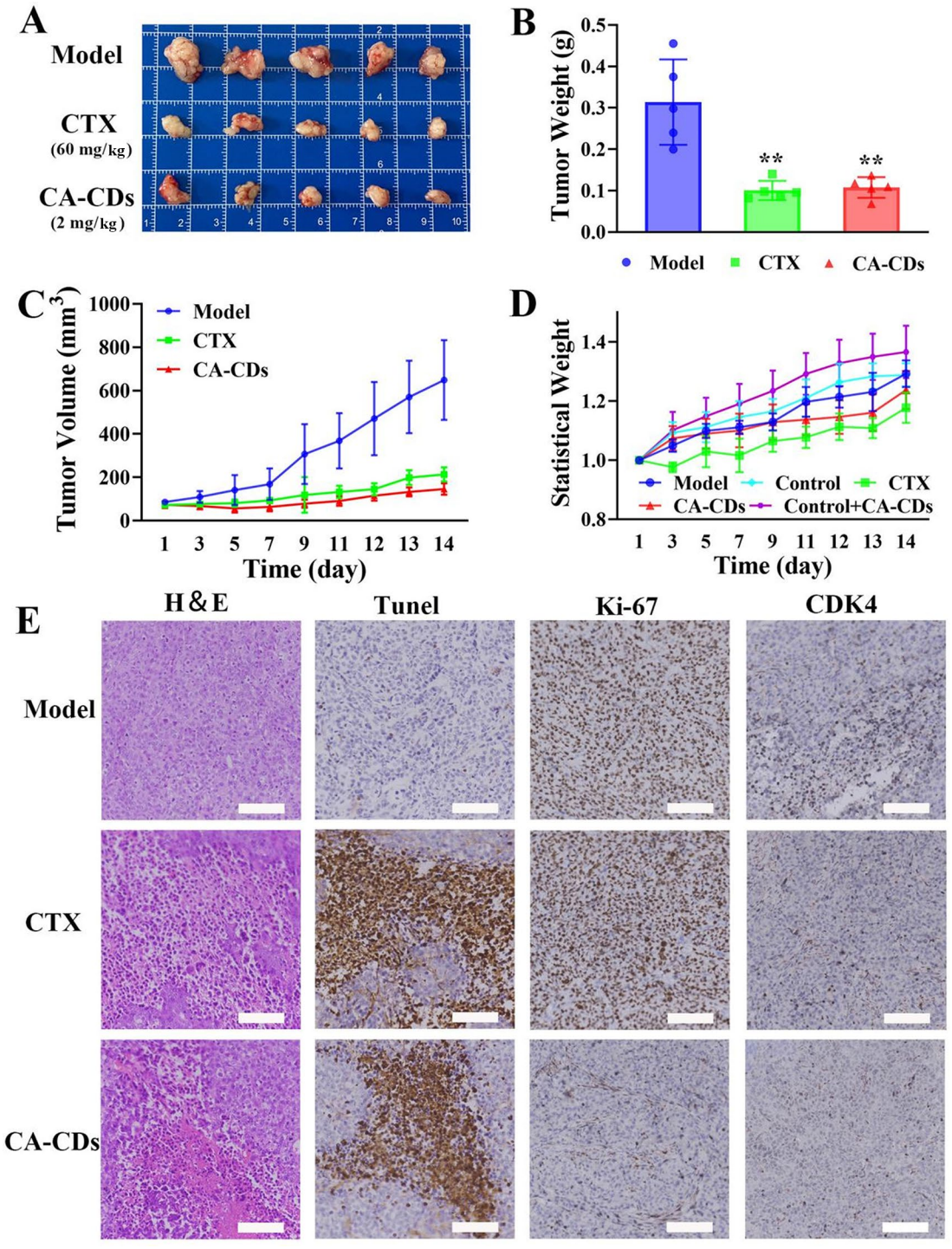

Fig. 6 Inhibitory effect of the CA-CDs on human papillary thyroid tumors in vivo. (**A**) Tumor images of the mice in the Model group, CTX group and CA-CDs group. (**B**) Statistic column chart of tumor weight of the mice in Model group, CTX group and CA-CDs group mice on the 14th day. (**C**) Statistic chart of tumor volume of the mice in Model group, CTX group and CA-CDs group mice from 1 to 14 days. (**D**) The calculated statistic chart of body statistical weight of mice in the Model group, Control group, CTX group, CA-CDs group and Control + CA-CDs group from 1 to 14 days. (**E**) H&E staining, Tunel staining, and immunohistochemical staining of tumor marker proteins (Ki-67 and CDK4) of mouse tumors in Model group, CTX group and CA-CDs group. The scale bars were 500 μm. *$p < 0.05$; **$p < 0.01$; ***$p < 0.001$ compared to Model

Conclusion

In conclusion, a new CA-CDs have been rapidly prepared by a hydrothermal method using caffeic acid, a natural plant active ingredient as the only reactant. The size of the prepared CA-CDs was relatively uniform, and they had good fluorescence properties, good salt tolerance and photobleaching resistance. The construction of carbon nanodots could effectively improve the bioabsorption rate and the efficacy of the anticancer drug. In vitro cell experiments showed that the CA-CDs had a significant inhibitory effect on the growth of the BCPAP cells. At a low concentration of 16 μg/mL of the CA-CDs, the inhibition rate of human thyroid cancer cells BCPAP reached ~ 79%. The CA-CDs has been demonstrated to inhibit the viability and migration of the BCPAP cells, and could induce S phase arrest and apoptosis of the BCPAP cells. The entry of the CA-CDs into the BCPAP cells was obviously, and the uptake of cells was greatest at 24 h of co-incubation. After 48 h treatment of the BCPAP cells with the CA-CDs, transcriptomics analysis was performed between the CA-CDs group and the Control group. Compared with the Control group, 7596 differential genes were screened out in the CA-CDs group. Among them, 2783 genes were up-regulated and 4813 genes were down-regulated. In the WB analysis, compared with the Control group, the expression contents of KRAS, p-BRAF, p-MEK1 and p-ERK1/2 proteins in the CA-CDs group were significantly reduced. It was suggested that the CA-CDs could simultaneously inhibit the proliferation of the BCPAP cells and promote the apoptosis of BCPAP cells by inhibiting the expression of the continuous RAS–RAF–MEK–ERK proteins in the MAPK classical signaling pathway. In vivo experiments showed that the CA-CDs at low doses (2 mg/kg) could significantly inhibit the volume and weight of human papillary thyroid tumor in mice. The dose administered was much lower than that of the clinically positive drug CTX (60 mg/kg). The CA-CDs had little effect on mice body weight change, and low toxicity and side effects to the mice. H&E staining, Tunel staining and IHC staining showed that the CA-CDs promoted apoptosis and decreased cell proliferation in tumor tissues. CA-CDs can be regarded as a perspective nanodrugs for the clinical treatment of poorly differentiated papillary thyroid carcinoma in the future.

Supplementary Information

The online version contains supplementary material available at https://doi.org/10.1186/s12951-024-02792-y.

Supplementary Material 1

Acknowledgements

This work was supported by Jilin Province International Science and Technology Cooperation Project (Grant No. 20240402039GH), the China Scholarship Council Fund, Jilin Province Health Special Project (Grant No. Sczsy201605), and Jilin Province Health Science and Technology Capacity Improvement Project (Grant No. 2021JC093).

Author contributions

JW X: Methodology, Investigation, Writing – review & editing, Funding acquisition. MW S: Visualization, Writing—original draft, Data curation. XL L: Data curation. HR Z: Investigation. JF W: Data curation. LZ X: Visualization. YX J: Methodology, Funding acquisition, Supervision. GQ Z: Investigation, Visualization. W J: Investigation. M L: Visualization. YY Y: Conceptualization, Funding acquisition. YN J: Funding acquisition, Project administration, Supervision. All authors reviewed the manuscript.

Data availability

No datasets were generated or analysed during the current study.

Declarations

Ethics approval and consent to participate

All animal experimental procedures were conducted according to all relevant ethical regulations and were approved by the Animal Care & Welfare Committee of the Changchun University of Chinese Medicine and the Ethical approval number is 2023365.

Consent for publication

All authors have approved the manuscript and agree for the submission.

Competing interests

The authors declare no competing interests.

Received: 29 February 2024 / Accepted: 20 August 2024
Published online: 18 September 2024

References

1. Siegel RL, Miller KD, Fuchs HE, Jemal A. Cancer statistics. CA Cancer J Clin. 2022;72:7–33.
2. Chen WQ, Zheng RS, ;Baade PD, Zhang SW, Zeng HM, Bray F, Jemal A, Yu XQ, He J. Cancer statistics in China. CA Cancer J Clin. 2016;66:115–32.
3. Jemal A, Ward EM, Johnson CJ, Cronin KA, Ma JM, Ryerson AB, et al. Annual report to the nation on the status of cancer, 1975–2014, featuring survival. J Natl Cancer Inst. 2017;109.
4. Du LB, Li RH, Ge MH, Wang YQ, Li HZ, Chen WQ, He J. Incidence and mortality of thyroid cancer in China, 2008–2012. Chin J Cancer Res. 2019;31:144–51.
5. Wiltshire JJ, Drake TM, Uttley L. Systematic review of trends in the incidence rates of thyroid Cancer. Thyroid. 2016;26:1541–52.
6. Kushchayeva YS, Kushchayev SV, Wexler JA, Carroll NM, Preul MC, Teytelboym OM, Sonntag VKH, Van Nostrand D, Burman KD, Boyle LM. Current treatment modalities for spinal metastases secondary to thyroid carcinoma. Thyroid. 2014;24:1443–55.
7. Xu ST, Zhu XY, Huang W, Zhou YF, Yan DY. Supramolecular cisplatin-vorinostat nanodrug for overcoming drug resistance in cancer synergistic therapy. J Control Release. 2017;266:36–46.
8. Jiang YN, Zhang XJ, Xiao LZ, Yan RY, Xin JW, Yin CX, Jia YX, Zhao Y, Xiao CY, Zhang Z, Song W. Preparation of dual-emission polyurethane/carbon dots thermoresponsive composite films for colorimetric temperature sensing. Carbon. 2020;163:26–33.
9. Ehtesabi H, Hallaji Z, Nobar SN, Bagheri Z. Carbon dots with pH-responsive fluorescence:a review on synthesis and cell biological applications. Microchim Acta. 2020;187:1–18.
10. Li S, Li L, Tu HY, Zhang H, Silvester DS, Banks CE, Zou GQ, Hou HS, Ji XB. The development of carbon dots:from the perspective of materials chemistry. Mater Today. 2021;51:188–207.
11. Luo WK, Zhang LL, Yang ZY, Guo XH, Wu Y, Zhang W, Luo JK, Tang T, Wang Y. Herbal medicine derived carbon dots:synthesis and applications in therapeutics, bioimaging and sensing. J Nanobiotechnol. 2021;19:320.
12. Yang ZC, Wang M, Yong AM, Wong SY, Zhang XH, Tan H, Chang AY, Li X, Wang J. Intrinsically fluorescent carbon dots with tunable emission derived from hydrothermal treatment of glucose in the presence of monopotassium phosphate. Chem Comm. 2011;47:11615–7.

13. Liu X, Liu YL, Thakor AS, Kevadiya BD, Cheng JM, Chen ML, Li Y, Xu Q, Wu QH, Wu Y, Zhang GL. Endogenous NO-releasing Carbon nanodots for Tumor-specific gas therapy. Acta Biomater. 2021;136:485–94.
14. Bai YL, Zhao JJ, Zhang LL, Wang SL, Hua J, Zhao SL, Liang H. A Smart Near-Infrared Carbon dot-metal Organic Framework assemblies for Tumor Micro-environment-activated Cancer Imaging and Chemodynamic-Photothermal Combined Therapy. Adv Healthc Mater. 2022;11:e2102759.
15. Lim SY, Shen W, Gao ZQ. Carbon quantum dots and their applications. Chem Soc Rev. 2015;44:362–81.
16. Li YJ, Tang ZH, Pan ZY, Wang RG, Wang X, Zhao P, Liu M, Zhu YX, Liu C, Wang WC, Liang Q, Gao J, Yu YC, Li ZY, Lei BF, Sun J. Calcium-mobilizing properties of Salvia miltiorrhiza-derived Carbon dots Confer enhanced environmental adaptability in plants. ACS Nano. 2022;16:4357–70.
17. Dordevic L, Arcudi F, Cacioppo M, Prato M. A multifunctional chemical toolbox to engineer carbon dots for biomedical and energy applications. Nat Nanotechnol. 2022;17:112–30.
18. Lagos KJ, Buzza HH, Bagnato VS, Romero MP. Carbon-based materials in photodynamic and photothermal therapies applied to tumor destruction. Int J Mol Sci. 2021;23:22.
19. Jiang YN, Xiao LZ, Wang JF, Tian TH, Liu GC, Zhao Y, Guo JJ, Zhang W, Wang JW, Chen CB, Gao WY. Yan, B. Carbon nanodots constructed by ginsenosides and their high inhibitory effect on neuroblastoma. J Nanobiotechnol. 2023;21:244.
20. Kuang YL, Song MW, Zhou XC, Mi JQ, Zhang Z, Liu GC, Shen ZR, Liu ZQ, Chen CB, Wu MX, Zhao Y, Yang B, Jiang YN. Cefminox sodium carbon nanodots for treatment and bacterial detection of bloodstream infection. Chem Eng J. 2023;470:143988.
21. Zhang ML, Cheng JJ, Hu J, Lu J, Zhang Y, Lu F, Kong H, Qu HH, Zhao Y. Green Phellodendri Chinensis Cortex-based carbon dots for ameliorating imiquimod-induced psoriasis-like inflammation in mice. J Nanobiotechnol. 2021;19:105.
22. Yao L, Zhao MM, Luo QW, Zhang YC, Liu TT, Yang Z, Liao M, Tu PF, Zeng KW. Carbon Quantum dots-based Nanozyme from Coffee induces Cancer Cell Ferroptosis to activate Antitumor Immunity. ACS Nano. 2022;16:9228–39.
23. Liu YH, Xu BL, Lu MZ, Li SS, Guo J, Chen FZ, Xiong XL, Yin Z, Liu HY, Zhou DS. Ultrasmall Fe-doped carbon dots nanozymes for photoenhanced antibacterial therapy and wound healing. Bioact Mater. 2022;12:246–56.
24. Armendáriz-Barragán V, Zafar N, Badri W, Galindo-Rodríguez SA, Kabbaj D, Fessi H, Elaissari A. Plant extracts:from encapsulation to application. Expert Opin Drug Deliv. 2016;13:1165–75.
25. Ranoszek-Soliwoda K, Tomaszewska E, Małek K, Celichowski G, Orlowski P, Krzyzowska M, Grobelny J. The synthesis of monodisperse silver nanoparticles with plant extracts. Colloids Surf B. 2019;177:19–24.
26. Yu DS, Peng P, Dharap SS, Wang Y, Mehlig M, Chandna P, Zhao H, Filpula D, Yang K, Borowski V, Borchard G, Zhang Z, H, Minko T. Antitumor activity of poly(ethylene glycol)-camptothecin conjugate:the inhibition of tumor growth *in vivo*. J Control Release. 2005;110:90–102.
27. Pelinson LP, Assmann CE, Palma TV, da Cruz IBM, Pillat MM, Mânica A, Stefanello N, Weis GCC, Alve AD, de Andrade CM, Ulrich H, Morsch VMM, Schetinger MRC, Bagatini MD. Antiproliferative and apoptotic effects of caffeic acid on SK-Mel-28 human melanoma cancer cells. Mol Biol Rep. 2019;46:2085–92.
28. Ramos J. The regulation of extracellular signal-regulated kinase (ERK) in mammalian cells. Int J Biochem Cell Biol. 2008;40:2707–19.
29. Kim H, Bar-Sagi D. Modulation of signalling by Sprouty:a developing story. Nat Rev Mol Cell Biol. 2004;5:441–50.
30. Song YL, Bi ZF, Liu Y, Qin FR, Wei YQ, Wei XW. Targeting RAS-RAF-MEK-ERK signaling pathway in human cancer:current status in clinical trials. Genes Dis. 2023;10:76–88.
31. Karreth FA, Frese KK, DeNicola GM, Baccarini M, Tuveson DA. C-Raf is required for the initiation of lung cancer by K-Ras G12D. Cancer Discov. 2011;1:128–36.
32. Savoia P, Fava P, Casoni F, Cremona O. Targeting the ERK signaling pathway in melanoma. Int J Mol Sci. 2019;20:1483.
33. Uribe P, Andrade L, Gonzalez S. Lack of association between BRAF mutation and MAPK ERK activation in melanocytic nevi. J Invest Dermatol. 2006;126:161–6.
34. Fan YH, Ding HW, Kim D, Liu JY, Hong JY, Xu YN, Wang DP, Yang XS, Lee S. The PI3Kα inhibitor DFX24 suppresses Tumor Growth and Metastasis in Non-small Cell Lung Cancer via ERK inhibition and EPHB6 reactivation. Pharmacol Res. 2020;160:105147.
35. Bhamore JR, Jha S, Park TJ, Kailasa SK. Green synthesis of multi-color emissive carbon dots from Manilkara zapota fruits for bioimaging of bacterial and fungal cells. J Photochem Photobiol B Biol. 2019;191:150–5.
36. Godavarthi S, Kumar KM, Vélez EV, Hernandez-Eligio A, Mahendhiran M, Hernandez-Como N, Aleman M, Gomez LM. Nitrogen doped carbon dots derived from Sargassum fluitans as fluorophore for DNA detection. J Photochem Photobiol B Biol. 2017;172:36–41.
37. Lin CJ, Chang L, Chu HW, Lin HJ, Chang PC, Wang RYL, Unnikrishnan B, Mao JY, Chen SY, Huang CC. High amplification of the antiviral activity of Curcumin through Transformation into Carbon Quantum Dots. Small. 2019;15:e1902641.

Publisher's note